Cronfa - Swansea University Open Access Repository

_____

This is an author produced version of a paper published in:
Journal of Materials Chemistry C

_____

Cronfa URL for this paper:

_____

Paper:

_____

http://www.swansea.ac.uk/library/researchsupport/ris-support/

VO$_2$/TiO$_2$ Bilayer Films for Energy Efficient Windows with Multifunctional Properties

Işıl Top,[a,b]* Russell Binions,[a,b,§] Michael E. A. Warwick,[c] Charles W. Dunnill,[c] Marcin Holdynski [d] and Isaac Abrahams[b,e*]

[a]School of Engineering and Materials Science, Queen Mary University of London, Mile End Road, London E1 4NS, United Kingdom.

[b]Materials Research Institute, Queen Mary University of London, Mile End Road, London E1 4NS, United Kingdom.

[c]Energy Safety Research Institute, Swansea University, Bay Campus, Fabian Way, Swansea, SA1 8EN, United Kingdom.

[d]Institute of Physical Chemistry, Polish Academy of Sciences, ul. Kasprzaka 44/52, 01-224 Warsaw, Poland.

[e]School of Biological and Chemical Sciences, Queen Mary University of London, Mile End Road, London E1 4NS, United Kingdom.

[*]Authors to whom correspondence should be addressed

Email: i.top@qmul.ac.uk; tel: +44 (0) 20 7882 5305

Email i.abrahams@qmul.ac.uk; tel: +44 (0) 20 7882 3235

[§]Deceased

Abstract

Vanadium dioxide/titanium dioxide bilayer films have been investigated as a thermochromic coating for application as intelligent window glazings for buildings. The nanostructured VO_2 and TiO_2 films were deposited on fluorine doped tin oxide coated glass substrates using electric field assisted aerosol assisted chemical vapour deposition (ElFi-AACVD) and sol-gel spin coating, respectively. Their thermochromic properties were investigated using scanning electron microscopy, X-ray diffraction, variable temperature UV/Vis/NIR and X-ray photoelectron spectroscopies. Compared to bare VO_2 films, the VO_2/TiO_2 bilayer films exhibit an increase in visible light transmittance of up to 30%, an increase in integrated luminous transmisttance, with values up to 66%, and a higher transmittance modulation in the near infrared of up to 20% at the thermochromic transition temperature. The TiO_2 top layer not only enhances visible light transmittance, but also serves to protect the VO_2 bottom layer from oxidation. The bilayer films are shown to exhibit photo-induced super-hydrophilicity. These properties are affected by the morphology of the VO_2 under-layer.

1. Introduction

World-wide total energy consumption has dramatically increased over the last few decades, reaching 9384 Mtoe in 2015.[1] It has been estimated that around 40% of this energy consumption is attributable to temperature and humidity control of buildings, including air conditioning and heating.[2] One of the most important considerations in reducing energy consumption in buildings is the window glazing. Intelligent glazing systems with spectrally selective properties are seen as a practical and innovative method of controling the throughput of visible and solar thermal energy entering and leaving buildings, allowing for significant energy savings.[3]

Thermochromic glazings are designed to intelligently control the amount of light and heat (mainly in the near infra-red region) that can pass through the glazing as a function of the glazing temperature.[4,5] Vanadium dioxide (VO_2) exhibits a sharp change in optical properties around a thermochromic transition temperature (T_c) of 68 °C, which is associated with a semiconductor to metal transition, from a low-temperature monoclinic phase to a high-temperature tetragonal rutile-type phase.[6-8] For this reason, vanadium dioxide based thin films have been extensively investigated as possible smart-window coatings. On heating, the transmittance in the near infra-red (NIR) region decreases significantly at T_c, while there is no significant change in transmittance in the UV/Vis region.

Thermochromic performance is characterised by ΔT, the percent transmittance modulation between the cold and hot stage:[5]

$$\Delta T = T_{\text{cold}} - T_{\text{hot}} \tag{1}$$

Wavelength integrated luminous transmittance T_{lum} and solar transmittance, T_{sol} are given by:[9]

$$T_i = \frac{\int \varphi_i(\lambda) T(\lambda) \, d\lambda}{\int \varphi_i(\lambda) \, d\lambda} \tag{2}$$

where i denotes luminous or solar, $T(\lambda)$ denotes the transmittance at wavelength λ, $\varphi_{\text{lum}}(\lambda)$ is the photophic spectral sensitivity of the light-adapted eye (CIE (2008) physiologically-relevant 2-deg V(λ) luminous efficiency functions), and $\varphi_{\text{sol}}(\lambda)$ is the solar irradiance spectrum for air mass 1.5 corresponding to the sun at 37° above the horizon (ASTM G173-03 reference

spectrum, direct radiation + circumsolar). The solar modulation ΔT_{sol} can be calculated by substitution of the T_{sol} values (from equation 2) into equation 1.

Whilst VO_2 shows promise as a thermochromic material, its practical applicability is limited by a number of factors, *viz.*: its high T_c value of 68 °C, that ideally needs to be closer to room temperature;[10] a wide thermal hysteresis around T_c, ideally the change in transmittance at T_c should be large with no hysteresis;[11] generally poor visible light transmittance (T_{vis}) and poor glazing aesthetics (films exhibit a strong brown colour).[12,13]

Much research effort has gone into lowering the T_c value of VO_2 films, for example through doping with high-valence transition metal cations, such as Nb^{5+}, Ta^{5+}, Mo^{6+}, W^{6+} and Ru^{4+}.[14-19] Even though doping has been found to be effective in lowering T_c, it is still difficult to both lower T_c and increase visible light transmittance, as well as reducing thermal hysteresis.[20] Porosity has been demonstrated to have a positive effect on visible light transmittance in tungsten doped VO_2 films with low T_c values.[21,22] Another way of tuning T_c is to control the crystallite size within the VO_2 films.[23] Reduction in the crystallite and particle size causes strain, resulting in a lowering of T_c.[24] For this reason, nanostructured VO_2 films are of specific interest.[25] For example, a T_c of 29 °C was obtained in sol-gel deposited VO_2 films, with average crystallite sizes between 20-50 nm.[23] Warwick *et al.*[26-28] used a novel method for controlling film morphology, through deposition of VO_2 films with aerosol assisted chemical vapour deposition (AACVD) in the presence of an electric field. Increasing electric field strength was shown to reduce the average crystallite size and lower T_c. Higher electric fields are thought to cause the precursor to approach the surface with greater kinetic energy, allowing for faster nucleation. However, one problem with smaller crystallite size is that it leaves films more prone to oxidation, accompanied by an irreversible colour change and the complete loss of thermochromic properties.[27]

A convenient approach to overcome the issue of vulnerability to oxidation, is the use of protective layers of high refractive-index dielectric compounds.[29] These not only serve to provide protection against chemical attack[30] and excessive heat and humidity,[31] but also improve visible light transmittance, as well as allowing for other properties such as self-cleaning ability.[32-34] TiO_2 over-layers have been shown to be particularly effective in multilayer films with VO_2,[30,35,36] improving visible light transmittance, whilst maintaining good thermochromic properties. In addition, TiO_2 has proved to be an excellent photocatalyst for degradation of organic materials, allowing multilayer films to possess self-cleaning properties.

In the present work, the properties of VO_2/TiO_2 bilayer films produced using a novel combination of electric field assisted AACVD (ElFi-AACVD) and sol-gel spin coating are investigated. The resulting films show enhanced visible light transmittance and good transmittance modulation in NIR, in combination with photo induced superhydrophilicity.

2.   Experimental

2.1 Thin Film Preparation

VO_2 thin films were deposited using ElFi-AACVD. The reaction chamber was fitted with electrodes which allowed for an electric field to be applied during deposition. Reactions were carried out in a quartz cold walled reactor, as described previously.[26-28] Films were deposited on fluorine doped tin oxide (FTO) coated glass substrates (Pilkington) of dimensions 90 mm × 45 mm × 4 mm, which were washed with acetone (Sigma-Aldrich) and isopropyl alcohol (Sigma-Aldrich), sonicated in deionized water for 10 min and dried in flowing N_2 prior to use. A 0.1 M solution of $VO(acac)_2$ (0.384 g, Sigma-Aldrich, 99.99%) in ethanol (15 ml, Sigma-Aldrich) was used as the VO_2 precursor. Aerosols were formed using an ultrasonic humidifier, with nitrogen (BOC, 99.99%) as a carrier gas, at a flow rate of 1.5 L min^{-1}. The reaction chamber was heated to 440 °C using a graphite block, containing a Whatman heating cartridge, with temperature gradients of up to 50 °C between the top plate and the substrate. The substrate temperature was monitored using Pt–Rh thermocouples. VO_2 depositions were carried out for 15 min.

Three different electric field types were investigated: (1) DC-positive bias, where a DC potential was applied with a positive bias on the bottom plate; (2) DC-negative bias, where a DC potential was applied with a negative bias on the bottom plate; (3) AC, where an alternating current was applied on the bottom plate. The top and bottom plates were separated by 1 cm, allowing the precursor vapour and carrier gas to pass between them. The electric field strength used to produce VO_2 films was 1500 V m^{-1}. Table 1 summarises the films produced. The following notation is used to describe the plain VO_2 films: V0 denotes VO_2 films produced without the presence of an electric field, Vdc+15 and Vdc-15 denote bare VO_2 films produced when positive and negative biases were applied, respectively. Vac15 denotes samples produced under AC voltage.

The VO$_2$ coated substrate plates were cut into 2 cm × 2 cm pieces in preparation for deposition of the TiO$_2$ top layers. TiO$_2$ top layers were deposited in air using sol-gel spin coating as described elsewhere.[37] Titanium IV-butoxide (17.02 ml, Sigma-Aldrich, 97%) was added dropwise to a mixture of pentane-2,4-dione (2.567 ml, Sigma-Aldrich, 99%) in butan-1-ol (32 ml, 0.35 mol, Sigma-Aldrich, 99.4%), with continuous stirring for 30 min, resulting in a yellow solution. To this solution, a mixture of distilled water (3.6 ml, 0.2 mol) and propan-2-ol (9.04 g, 0.15 mol, Sigma-Aldrich, 99%) was added dropwise, with stirring, to hydrolyse the titanium precursor. The solution was stirred for a further 30 min, and left to gel for 2 h. In each case, the resulting gel was added dropwise onto a VO$_2$ film, which was spun at 1000 rpm for 30 s, followed by 3000 rpm for 40 s. The films were subsequently annealed at 500 °C, under flowing N$_2$ (1 litre min^{-1}) for 1 h. Bilayer films are denoted as VT in Table 1.

2.2   General Characterisation

Sample adhesion was tested using the standard Scotch tape test, as well as attempted abrasion using tissue paper and brass and steel styli. Surface morphology was examined by scanning electron microscopy (SEM), using an FEI Inspect F Field Emission SEM at an accelerating voltage of 10 keV, a spot size of 3 nm and a working distance of 10 mm. X-ray powder diffraction (XRD) measurements were made on a PANalytical X'Pert Pro diffractometer fitted with an X'Celerator detector in glancing angle ($\alpha = 3°$) mode, using Ni filtered Cu-Kα radiation. The diffraction patterns were collected over the 2θ range 20–70°, with a step size of 0.033° and an effective count time of 1.7 s per step. X-ray photoelectron spectroscopy (XPS) measurements were performed using a VG Scientific ESCALAB-210 spectrometer, with Al-Kα non-monochromated radiation (1486.6 eV; 300 W) as the excitation source. The pressure during analysis was 5.0×10^{-9} mbar. The binding energies of the target elements (V 2p, Ti 2p) were determined at a pass energy of 25 eV, using the binding energy of carbon (C 1s: 284.8 ± 0.2 eV) as a reference. A Shirley background[38] subtraction was applied to obtain the XPS signal intensity. Data were corrected for surface charging effects, prior to fitting using an asymmetric Gaussian/Lorentzian function.

2.3   Thermochromic Activity

UV/vis/NIR transmission spectra were measured using a Lambda 950 UV–Vis–NIR spectrometer over the wavelength range 300–2500 nm with an air spectral background. In order to determine the thermochromic properties of the films, transmission was recorded above and below T_c by heating the samples on a hot plate. Hysteresis data were obtained for films by heating between *ca*. 20 °C and 80 °C, using a custom-built heated sample holder. Spectra were recorded at 5 °C intervals on heating and cooling. T_c was measured as the mid-point of the hysteresis loop.

2.4   Water Droplet Contact Angle

Photo-induced super-hydrophilicity (PSH) was measured through changes in the contact angle of a water droplet on the film surface upon UV irradiation. The samples were irradiated for 30 min in a custom-built light box using a 32 W UVITEC UV lamp, with a main emission wavelength of 254 nm and an incident light intensity of 15 μW cm^{-2}. In each case, a 3 μl droplet of deionised water was placed on the film surface. The diameter of the drop was then measured after it had settled. Measurements were performed on a Goniometer Kruss DSA100 drop shape analyser, using digital images to record droplet base length and height, from which the contact angles were calculated. If a coating shows PSH after UV irradiation, the water droplet will be seen to spread out with a very low contact angle. Contact angles were measured prior to and post UV irradiation.

3. Results and Discussion

3.1 Crystalline Structure and Physical Properties

All the VO_2 films produced were translucent brown in colour, typical of these films.[26-28] The films could not be wiped away with tissue, and passed the Scotch tape test. They could not be removed with a brass stylus, but they could be damaged using a steel stylus. VO_2/TiO_2 bilayer films were lighter in colour compared to the bare VO_2 films and showed good transparency (Fig. 1). These VO_2/TiO_2 bilayer films also showed good adherence to the substrate, passing the tissue and Scotch-tape tests. They were additionally resistant to damage from both brass and steel styli.

The XRD patterns of representative films are shown in Fig. 2 and are dominated by peaks from the FTO coating of the glass substrate. In the single layer VO_2 films, peaks attributable to VO_2 are observed and are indicated in Fig. 2, but from the data it is impossible to distinguish between the tetragonal (JCPDS # 44-253) and monoclinic (JCPDS # 33-1441) forms of VO_2, due

to the weakness of diffraction from this layer. In the XRD patterns of the VO_2/TiO_2 bilayer films, peaks associated with the VO_2 under-layer are not visible and only the (101) reflection of anatase TiO_2 (JCPDS # 21-1272) is evident at about 27.6° 2θ, along with peaks from the FTO coating of the substrate.

3.2 Surface Morphology

Fig. 3 shows SEM images of bare VO_2 films prepared under different deposition conditions, as summarised in Table 1. In the absence of an applied field (V0), the surface morphology of the film is comprised of small nanoparticles (~30 nm in diameter), which are coalesced to form randomly aligned larger grains, typical of AACVD deposited VO_2 films.[26-28,39] For films produced in the presence of an electric field, there are significant changes in the surface morphology. For films deposited under a positive DC bias (Vdc+15), the surface is formed of smaller particles, with sizes in the range of 25-30 nm. The films produced under a negative bias DC field (Vdc-15) were found to be formed of clusters (*ca*. 140 nm in diameter) of small particles (~10 nm in diameter), similar to those observed at zero applied field, but with a larger grain size and higher porosity. VO_2 films, produced in an AC field (Vac15), where the polarity alternates during the deposition, show characteristics similar to those produced under positive and negative DC biases, consisting of clusters of small particles (10 nm in diameter), but with less porosity than seen under negative DC bias. The results are consistent with those previously reported.[26-28]

Fig. 4 shows SEM images of VO_2/TiO_2 bilayer films. The surface morphologies of the films are similar to each other and show a smooth and less complex structure compared to the bare VO_2 films, which is more typical of sol-gel prepared films.[40] Particle sizes are in the order of 5 nm. The VT0 film, where the VO_2 under-layer was deposited in the absence of an electric field, has a non-uniform, loose morphology, which is likely caused by solvent evaporation during the annealing step, leaving a cracked surface. Additionally, the irregular surface morphology of the VO_2 under-layer (Fig. 3) could have a significant effect on the TiO_2 top-layer, leaving randomly aligned grains. Similarly, the VTdc+15 film, which had a VO_2 under-layer deposited under positive DC bias, also exhibited an irregular surface, but with a greater extent of cracking and corresponds to the film where the VO_2 under-layer had the lowest porosity. A much better surface coverage was obtained for the VTdc-15 film, where

the VO_2 under-layer was produced under negative DC bias. This film exhibited complete crack-free surface coverage. A similar surface morphology was observed for the VTac15 film, showing complete surface coverage made up of agglomerations of small nanoparticles (~5 nm in diameter). Overall, the SEM results confirm good surface coverage by TiO_2, with the porosity and morphology of the VO_2 under-layer exhibiting an influence on that of the top-layer.

3.3 Thermochromic Properties

UV-Vis-NIR spectroscopy was used to measure visible light transmittance (T_{vis}), transmittance modulation (ΔT) in the NIR region and the critical transition temperature (T_c). Above 1300 nm, the optical properties of all films were dominated by those of the FTO coated glass substrate, which exhibits strong absorption of NIR radiation. Fig. 5 shows the spectral changes in the UV-Vis-NIR transmittance for the studied bare VO_2 and VO_2/TiO_2 bilayer films between room temperature and 80 °C. All VO_2/TiO_2 bilayer films showed an increase in transmittance of *ca.* 20 to 30% in the visible (T_{vis}) region at both temperatures, compared to the corresponding bare VO_2 films, in agreement with previous work on sputtered VO_2/TiO_2 films.[34,36] The maximum T_{vis} value for the bilayer VO_2/TiO_2 films was 79% for the VTdc+15 sample and corresponds to the film with the least porous VO_2 under-layer and lowest particle size. Films with the VO_2 layer deposited under AC field showed significantly lower T_{vis} values than other films (*ca.* 45%, for Vac15 increasing to *ca.* 62% for VTac15). The correlation between increasing T_{vis} and porosity has been noted before in W doped VO_2 films.[21,22]

As seen in Fig. 5, all samples showed thermochromic behaviour, with a decrease in transmittance at 80 °C. The maximum transmittance modulation between room temperature and 80 °C occurs at around 1100 nm and therefore, ΔT values and hysteresis plots were obtained from the data collected at this wavelength. All films showed some degree of transmittance modulation (ΔT) at 1100 nm between the cold and hot stages, ranging from 2.0% for the Vdc-15 sample to 21.7% for the VTdc+15 sample. Integrated luminous transmittance and solar modulation values for the films are tabulated in Table 2. The bare VO_2 films exhibited higher T_{lum} values than those for films produced by sputtering,[34] and sol-gel methods.[41] ΔT_{sol} values of the bare VO_2 films varied between 1.3 and 7.7, comparable to similar nanostructured films prepared by other methods.[9,13]

The presence of a TiO$_2$ over-layer is seen to increase T_{lum} significantly in all films, with small differences in ΔT_{sol} between the bare VO$_2$ and the corresponding bilayer films. This increase in T_{lum} with TiO$_2$ coating has previously been observed in bilayer films produced by various other techniques. For instance, T_{lum} values increased from 32% to 47% in films produced by RF sputtering,[34] while for sol-gel produced films more modest increases from 42 to 47 % [12] and from 39% to 44 % are observed.[9] Thus the T_{lum} increases seen in the present study are exceptionally high.

Higher values for T_{lum} have been reported, for example Chen *et al.*[13] obtained a value of 84.8% for T_{lum}, with TiO$_2$ over-layers, but with a ΔT_{sol} of only 0.9%. Indeed, it has been reported that it is difficult to achieve improvements in both T_{lum} and ΔT_{sol} and that it is often the case of a compromise between higher T_{lum} and slightly lower ΔT_{sol} [13,34,42] In the present study, the observed ΔT_{sol} values are comparable with those in other studies. [20, 32, 36]

The evolution of transmittance as a function of temperature was characterised through hysteresis plots at 1100 nm. Fig. 6 shows a comparison between the hysteresis plots of the bare Vdc+15 and the bilayer VTdc+15 films. Significant hysteresis between heating and cooling is evident in the bare VO$_2$ film, as previously reported.[43] The introduction of the TiO$_2$ top layer causes a significant reduction in the hysteresis loop width to around 10 °C and a reduction of the T_c value from *ca.* 59 °C to *ca.* 46 °C. However, there is also a significant reduction in % transmittance at 1100 nm from 47% to 33% for the bare VO$_2$ and TiO$_2$ coated films, respectively.

The observed reduction of T_c in the VO$_2$/TiO$_2$ bilayer films may be due to slight deviations in stoichiometry of the VO$_2$ layer caused by diffusion of titanium from the TiO$_2$ top-layer during annealing.[44] This doping phenomenon would be enhanced by the porosity of the VO$_2$ under-layer.[27] Ti^{4+} doping would introduce oxide ion vacancies which disrupt the zigzag chains of the V-V pairs, characteristic of the low-temperature phase, resulting in a decrease of T_c.[30] Similar observations had been made previously in VO$_2$/WO$_3$ and VO$_2$/SiO$_2$ multilayer films.[45,46] Another potential factor is the additional strain on the VO$_2$ layer caused by lattice mismatch with the TiO$_2$ top-layer, leading to a beneficial extra reduction in T_c. This strain induced reduction in T_c has been reported in VO$_2$/SiO$_2$/TiO$_2$ [47] and TiO$_2$/VO$_2$/TiO$_2$ multilayer films.[27,48]

3.4 Thermal Protection

In addition to increasing the visible light transmittance and NIR transmittance modulation, TiO_2 over-layers have been shown to work as thermal protection layers.[49,50] In our previous work, we reported that, the application of electric fields caused a reduction in the crystallite and particle sizes, which leads to a higher NIR transmittance modulation and lower T_c, compared to films produced in the absence of electric fields.[26-28,51] However, the smaller particle size leaves the VO_2 films susceptible to oxidation on thermal cycling, resulting in an irreversible loss of thermochromic properties. The results of the present study are reproducible over three cycles of heating and cooling up to 80 °C, confirming the protective role of TiO_2 in these bilayer systems. In order to assess the extent of thermal oxidation protection offered by the TiO_2 top-layers, previously cycled bilayer films were examined by XPS. Fig.7 shows XPS spectra for selected samples with binding energies summarised in Table 3. All spectra showed a characteristic Ti $2p_{3/2}$ and $2p_{1/2}$ doublet. The Ti $2p_{3/2}$ binding energy showed no significant variation between samples, with a value typical for TiO_2.[52] In the case of vanadium, interpretation is complicated by the closeness of the strong O1s peak. The V $2p_{3/2}$ $2p_{1/2}$ doublet is seen in all but the sample with the VO_2 layer prepared in an AC field. The V $2p_{3/2}$ binding energies are typical for V^{4+} and comparable to previously reported values for VO_2.[53] Analysis of the vanadium peaks is complicated by the presence of strong single peaks evident at 517.7 eV and 519.2 eV. All attempts at fitting these peaks to additional vanadium $2p_{3/2}$ $2p_{1/2}$ doublets were unsuccessful and their position at *ca*. 10 and 12 eV below the O1s peak (at *ca*. 530 eV) suggests that they are in fact satellites of this peak. The results therefore appear to confirm the effectiveness of TiO_2 as a protective layer preventing oxidation on thermal cycling.

3.5 Wettability

Photoactive TiO_2 films often demonstrate photo-induced super-hydrophilicity (PSH). The degree of PSH can be monitored by observing the change in the contact angle of a water droplet on the film surface upon UV illumination. A wavelength of 254 nm (4.88 eV) was selected to ensure the radiation had a greater energy than the band gap of TiO_2 (3.2 eV). Fig. 8 shows photographs of water droplets on the surface of the studied bilayer films prior to and post UV irradiation for 60 min. As shown in Table 4, the measured contact angle decreased in all cases after irradiation, with that for the VTdc+15 showing the greatest reduction from 72° to

9°, significantly better than seen for the film where the VO_2 under-layer was prepared in the absence of an electric field (VT0). The observed PSH behaviour is consistent with studies of plain TiO_2 films, which exhibit PSH after UV irradiation.[54,55] The PSH effect in TiO_2/VO_2 multi-layer films has been attributed to the creation of oxide ion vacancies (and associated reduction of Ti) at the surface by the UV radiation, leading to sites that are attractive to water molecules and rendering the surface with greater hydrophilicity. However, Takeuchi *et al.*[56] have suggested that heating effects caused by the UV irradiation are more important and lead to a decrease in surface tension within the water droplets. In fact the effect of temperature on surface tension is well known and for a liquid in equilibrium with its vapour can be described by:

$$\gamma = \gamma_0 \left(1 - \frac{T}{T_c}\right)^n \tag{3}$$

where T is the temperature in K, T_c is the critical temperature when surface tension vanishes and γ_0 and n are constants for a particular liquid. While, surface morphology and in particular porosity are very likely to influence surface tension, the observed variation of PSH behaviour between samples, suggests an influence of the VO_2 under-layer morphology, rather than that of the TiO_2 top layer, with the films with the least porous VO_2 under-layers showing the strongest PSH effect. This may be attributable to the extent of the interfacial region formed between the VO_2 under-layer and the TiO_2 top layer, with the films with the most porous VO_2 under-layers likely to exhibit larger interfacial regions with TiO_2 penetrating more extensively during top-layer deposition. While this is expected to have little influence on oxide ion vacancy creation at the TiO_2 surface, the improvement of heat flow from the TiO_2 layer to the VO_2 under-layer could lead to a reduced thermal effect from the UV radiation at the TiO_2 surface.

4. Conclusions

The electric field modulated AACVD reaction of $VO(acac)_2$ at 440 °C resulted in the deposition of thin films of nano-structured VO_2 on FTO coated glass substrates, with complex and porous surfaces. TiO_2 layers were deposited on the VO_2 films by sol-gel spin coating followed by annealing at 500 °C. These TiO_2 top-layers increased visible light transmittance as well as increased T_{lum} by as much as 50% in some cases, with a small sacrifice in the solar modulation values compared to the corresponding bare VO_2 films. Application of TiO_2 top-

12

layers resulted in reduced NIR transmittance hysteresis, as well as a lowering of T_c. The best results were obtained for VTdc+15, where the VO_2 under layer was produced under the application of a positive DC bias, with a field strength of 1500 V m^{-1}, giving a T_c value of 46 °C, significantly lower than seen in previous studies of bare VO_2 films produced under electric fields, a ΔT at 1100 nm of 21.7%, with a reasonable integrated solar modulation, ΔT_{sol} of 4.3%.

Application of the TiO_2 top layer not only results in enhanced thermochromic properties, but also offers protection against oxidation of the thermochromically active VO_2 layer, improves the aesthetic appearance of the glazing and visible light transmittance, as well as providing enhanced wetting behaviour through PSH. The microstructure of the VO_2 under-layer is found to influence the PSH behaviour of the bilayer films, with the least porous VO_2 under-layers showing the strongest PSH effect. The higher porosity of the films allows for greater penetration of the TiO_2 top layer generating a larger interfacial region, with better heat flow between the TiO_2 top layer and the VO_2 under-layer. This might account for the smaller PSH effect in samples with high VO_2 layer porosity by reducing the heating effect of the UV source at the TiO_2 surface. PSH is an important consideration in extensively glazed structures and combined with the known property of photocatlytic degradation of simple organic molecules by TiO_2 films, gives the glazing self-cleaning properties. These bilayer structures, made by a unique combination of ElFi-AACVD and sol-gel spin coating offer a simple and versatile way of producing durable window coatings with enhanced properties, affording the design and integration of advanced thermochromic structures with controllable functionalities for intelligent windows.

Conflicts of interest

There are no conflicts of interest to declare.

Acknowledgements

References

1. The International Energy Agency, *Key World Energy Statistics*, 2017, 6.

2. A. M. Omer, *Renew. Sustain. Energy Rev.,* 2008, **12**, 2265–2300.

3. S. B. Sadineni, S. Madala and R. F. Boehm, *Renew. Sustain. Energy Rev.,* 2011, **15**, 3617–3631.

4. M. Kamalisarvestani, R. Saidur, S. Mekhilef and F. S. Javadi, *Renew. Sustain. Energy Rev.*, 2013, **26**, 353–364.

5. A. L. Anderson, S. Chen, L. Romero, I. Top and R. Binions, *Buildings*, 2016, **6,** 37.

6. F. J. Morin, *Phys. Rev. Lett.*, 1959*,* **3**, 34–36.

7. C. O. F. Ba, S. T. Bah, M. D'Auteuil, V. Fortin, P. V. Ashrit and R. Vallee, *Curr. Appl. Phys.*, 2014, **14**, 1531–1537.

8. J. B. Goodenough, *J. Solid State Chem.,* 1971, **3**, 490–500.

9. C. Liu, S. Whang, Y. Zhou, H. Yang, Q. Lu, D. Mandler, S. Magdassi, C. Y. Tay and Y. Long, *J. All. Comp.*, 2018, **731**, 1197-1207.

10. H. Ye, X. Meng, and B. Xu, *Energy Build.*, 2012, **49**, 164–172.

11. M. E. A. Warwick, I. Ridley, R. Binions, *Energy Build.*, 2014, **77,** 80–90.

12. M. Saeli, C. Piccirillo I. P. Parkin, R. Binions, and I. Ridley, *Energy Build.* **42**, 2010, 1666–1673.

13. Z. Chen, Y. Gao, L. Kang, J. Du, Z. Zhang, H. Luo, H. Miao and G. Tan, *Sol. Energy Mater. Sol. Cells*, 2011, **95**, 2677–2684.

14. K. Miyazaki, K. Shibuya, M. Suzuki, H. Wado and A. Sawa, *Jpn. J. Appl. Phys.*, 2014, **53**, 071102.

15. L. Jinhua, Z. Daohua, W. Yan, Z. Meng, Z. Weifeng and Yuan, Ningyi, *IPGC 2008 IEEE Photonics Global@Singapore,* 2008, 1-4.

16. T. Manning, I. Parkin, C. Blackman and U. Qureshi, *J. Mater. Chem.*, 2005, **2**, 4560–4566.

17. G. Pan, J. Yin, K. Ji, X. Li, X. Cheng, H. Jin and J. Liu, *Sci. Rep.*, 2017, **7**, 1–11.

18. C. Batista, R. M. Ribeiro, and V. Teixeira, *Nanoscale Res. Lett.* 2011, **6**, 301.

19. C. Piccirillo, R. Binions, I. P. Parkin, *Thin Solid Films*, 2008, **516**, 1992–1997.

20. I. Top, J. Schläfer, R. Binions, I. Papakonstantinou, S. Srimurugananthan, M. Powell, I. P. Parkin, C. J. Carmalt and I. Abrahams, *MRS Advances,* 2018*,* 1-7.

21. C. Zhao, H. Tao, F. Peng, R. Pan and X. Zhao, *J. Sol-Gel Sci. Technol.,* 2016, **78**, 582–588.

22. L. Hu, H. Tao, G. Chen, R. Pan, M. Wan, D. Xion and X. Zhao, *J. Sol-Gel Sci. Technol.*,

2016, **77**, 85–93.

23. B. Wang, S. Chen, Z. Huang and M. Fu, *Appl. Surf. Sci.* 2012, **258**, 5319–5322.

24. Z. Zhang, Y. Gao, Z. Chen, J. Du, C. Cao, L. Kang and H. Luo, *Langmuir*, 2010, **26**, 10738–10744.

25. Z. Huang, S. Chen, B. Wang, Y. Huang, N. Liu, J. Xu and J. Lai, *Thin Solid Films*, 2011, **519**, 4246–4248.

26. M. E. A. Warwick, I. Ridley and R. Binions,. *J. Nanosci. Nanotechnol.* 2011, **11**, 8158–8162..

27. M. E. A. Warwick and R. Binions, *Sol. Energy Mater. Sol. Cells*, 2015, **143**, 592–600.

28. A. J. T. Naik, C. Bowman, N. Panjwani, M. E. A. Warwick and R. Binions, *Thin Solid Films.*, 2013, **544**, 452-456.

29. J. Zhou, Y. Gao, Z. Zhang, H. Luo, C. Cao, Z. Chen, L. Dai and X. Liu, *Sci. Rep.*, 2013, **24**, 1–5.

30. J. Zheng, S. Bao, and P. Jin, *Nano Energy*, 2015, **11**, 136–145.

31. Y. X. Ji, S. Y. Li, Niklasson, G. A. and C. G. Granqvist, *Thin Solid Films*, 2014, **562**, 568–573.

32. A. Taylor, I. P. Parkin, N. Noor, C. Tummeltshammer, M. S. Brown and I. Papakonstantinou, *Opt. Express,* 2013, **21**, A750–A764.

33. M. E. A. Warwick, C. W. Dunnill and R. Binions, *Chem. Vap. Dep.*, 2010, **16**, 220–224.

34. P. Jin, G. Xu, M. Tazawa and K. Yoshimura, *Jpn. J. Appl. Phys.*, 2002, **41**, L278–L280.

35. U. Qureshi, T. Manning, and I. P. Parkin, *J. Mater. Chem.*, 2004, **14**, 1190–1194,

36. N. R. Mlyuka, G. A. Niklasson and C. G. Granqvist, *Sol. Energy Mater. Sol. Cells*, 2009, **93**, 1685–1687.

37. K. Page, R. G. Palgrave, I. P. Parkin, M. Wilson, M. Savin, L. P. Shelley and A. V. Chadwick, *J. Mater. Chem.,* 2007, **17**, 95–104.

38. D. A. Shirley, *Phys. Rev. B,* 1972, **5**, 4709–4714.

39. C. Piccirillo, R. Binions and I. P. Parkin, *Eur. J. Inorg. Chem.*, 2007, **2007**, 4050–4055.

40. S. Nadzirah, K. L. Foo, and U. Hashim, *Int. J. Electrochem. Sci.*, 2015, **10**, 5498–5512.

41. M. Wan, B. Liu, S. Wang, L. Hu, Y. He, H. Tao, X. Zhao, *J. All. Comp.,* 2017, **706**, 289-296.

42. N. R. Mlyuka, G. A. Niklasson and C. G. Granqvist, *Phys. Stat. Solidi A*, 2009, **9**, 2155-2160.

43. C. Piccirillo, R. Binions and I. P. Parkin, *Chem. Vap. Depos.* 2007, **13**, 145–151.

44. S. Zhang, I. S. Kim and L and J. Lauhon, *Nano Lett.*, 2011, **11**, 1443–1447.

45. S. Long, H. Zhou, S. Bao, Y. Xin, X. Cao and P. Jin, *RSC Adv.*, 2016, **6**, 106435.

46. J. Zhang, J. Wang, C. Yang, H. Jia, X. Cui, S. Zhao and Y. Xu, *Sol. Energy Mater.,* 2017, **162**, 134-141.

47. M. J. Powell, R. Quesada-Cabrera, A. Taylor, D. Teixeira, I. Papakonstantinou, R. G. Palgrave, S. Gopinathan and I. P. Parkin, *Chem. Mater.*, 2016, **28**, 1369–1376.

48. K. Okimura, T. Watanabe *and* J. Sakai, *J. Appl. Phys*., 2012, **111**, 073514.

49. P. Jin, G. Xu, M. Tazawa and K. Yoshimura, *Appl. Phys. A Mater. Sci. Process.*, 2003, **77**, 455–459.

50. Y. Li, S. Ji, Y. Gao, H. Luo and M. Kanehira, *Sci. Rep*. 2013, **3**, 1370.

51. M. Warwick, R. Smith, N. Furlan, J. Crane and R. Binions, *ECS Trans.*, 2010, **28**, 1–13.

52. M. C. Biesinger, L. W. M. Lau, A. R.Gerson and R. S. C. Smart, *Appl. Surf. Sci.* 2010, **257**, 887–898.

53. G. Silversmit, D. Depla, H. Poelman, G. B. Marin, R. De Gryse, *J. Electron Spectros. Relat. Phenomena*, 2004, **135**, 167–175.

54. L. Anderson, R. Binions, *Coatings*, 2014, **4**, 796–809.

55. N. Stevens, C. I. Priest, R. Sedev and J. Ralston, *Langmuir*, 2003, **19**, 3272–3275.

56. M. Takeuchi, K. Sakamoto, G. Martra, S. Coluccia and M. Anpo, *J. Phys. Chem. B.,* 2005, **109***, 15422-15428.

Table 1. Reaction conditions used for production of bare VO$_2$ and bilayer TiO$_2$/VO$_2$ films used in this study.

Sample Name	Voltage type	Applied voltage (V)	Film	Field Strength (V m^{-1})
V0	-	0	VO$_2$	0
VT0	-	0	VO$_2$/TiO$_2$	0
Vdc+15	DC (+)	15	VO$_2$	1500
Vdc-15	DC (-)	15	VO$_2$	1500
Vac15	AC	15	VO$_2$	1500
VTdc+15	DC (+)	15	VO$_2$/TiO$_2$	1500
VTdc-15	DC (-)	15	VO$_2$/TiO$_2$	1500
VTac15	AC	15	VO$_2$/TiO$_2$	1500

Table 2. Summary of thermochromic response of bare VO$_2$ and bilayer TiO$_2$/VO$_2$ films. Hot and cold stages are denoted by h and c.

Sample	$T_{lum.c}$	$T_{lum,h}$	$T_{sol,c}$	$T_{sol,h}$	ΔT_{sol}
V0	46.0	44.7	42.5	34.7	7.7
Vdc+15	46.5	45.3	40.5	36.3	4.1
Vdc-15	50.0	48.8	40.7	39.4	1.3
Vac15	40.0	43.4	32.8	30.0	2.7
VT0	63.8	63.8	60.6	55.2	5.4
VTdc+15	55.7	56.1	62.5	58.2	4.3
VTdc-15	66.0	65.4	61.9	58.1	3.8
VTac15	59.8	59.8	51.7	49.3	2.4

Table 3. Binding energies (eV) from XPS spectra for studied bilayer TiO$_2$/VO$_2$ films

Sample Name	V $2p_{3/2}$	V $2p_{1/2}$	Ti $2p_{3/2}$	Ti $2p_{1/2}$
VT0	516.5	523.4	459.1	464.7
VTdc+15	516.7	523.3	459.1	464.7
VTdc-15	516.7	524.2	459.1	464.7
VTac15	-	-	459.1	464.7

Table 4. Average contact angles (°) of VO$_2$/TiO$_2$ bilayer films before and after 60 min of UV irradiation.

| Sample	Before UV irradiation	After UV irradiation
VT0	63 ± 2	57 ± 3
VTdc+15	72 ± 3	9 ± 3
VTdc-15	49 ± 2	46 ± 2
VTac15	58 ± 2	10 ± 3

Figure captions

Fig. 1. Images of VO_2/TiO_2 bilayer films (a) VT0, (b) VTdc+15, (c) VTdc-15 and (d) VTac15.

Fig. 1. XRD patterns of bare VO_2 and bilayer VO_2/TiO_2 films. Peaks attributable to VO_2 (+), TiO_2 (-) and FTO (*) are indicated.

Fig. 3.SEM images of bare VO_2 films produced by ElFi-AACVD, under 0 and 1500 V m^{-1} field strengths, with positive DC bias, negative DC bias, and AC.

Fig. 4.SEM images of bilayer VO_2/TiO_2 films.

Fig. 5. UV-Vis spectra for bare VO_2 (dashed lines) and bilayer VO_2/TiO_2 (solid lines) films at room temperature (blue) and at 80 °C (red).

Fig. 6. NIR transmittance hysteresis plots recorded at 1100 nm for Vdc+15 and VTdc+15 films. Blue and red lines denote heating and cooling runs, respectively. The arrows denote the T_c values.

Fig. 7. Fitted vanadium XPS spectra for (a) VT0, (b) VTdc+15, (c) VTdc-15 and (d) VTac15 films. For data representation a Shirley-type background was subtracted.

Fig. 8. Images of water droplets on the surface of VO_2/TiO_2 bilayer films before and after 60 min of UV irradiation at 254 nm.
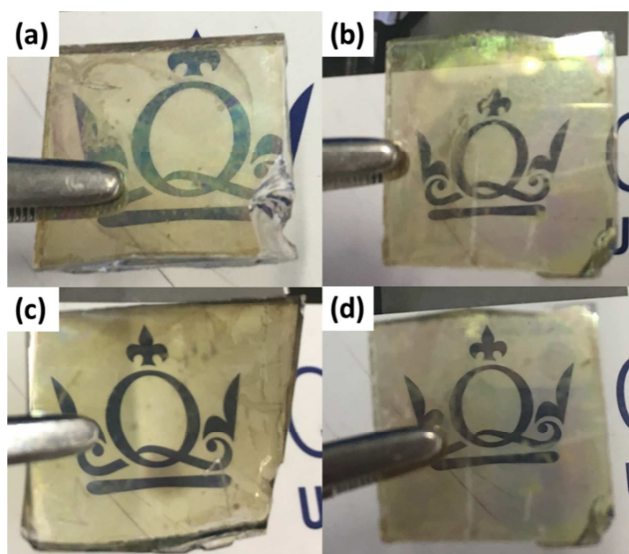
Fig. 1. Images of VO$_2$/TiO$_2$ bilayer films (a) VT0, (b) VTdc+15, (c) VTdc-15 and (d) VTac15.
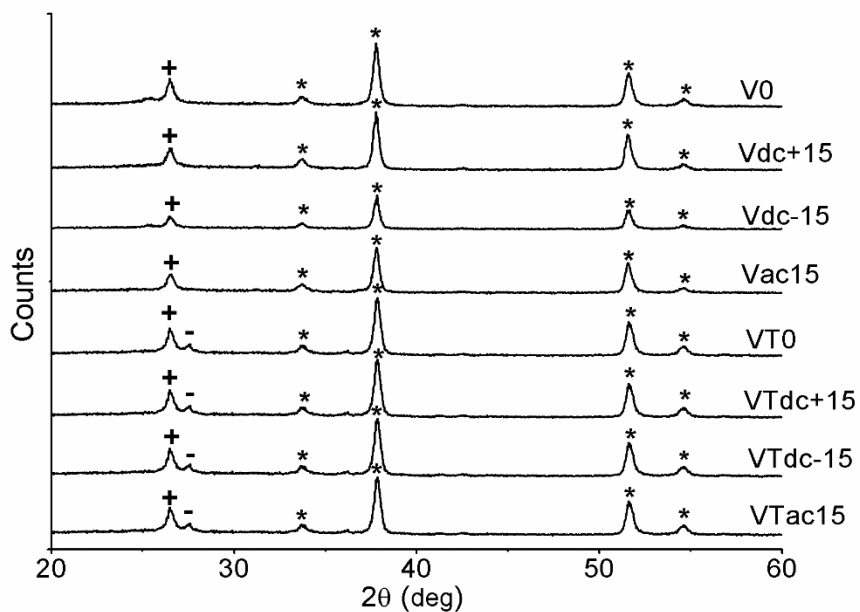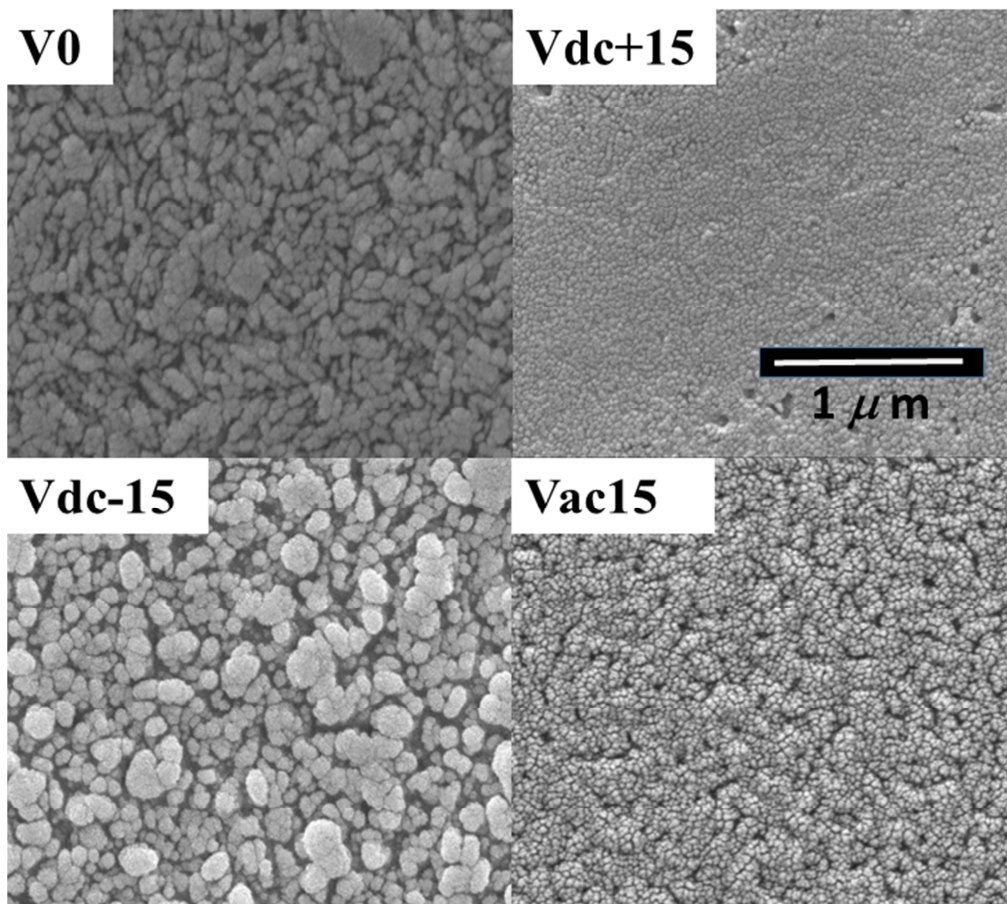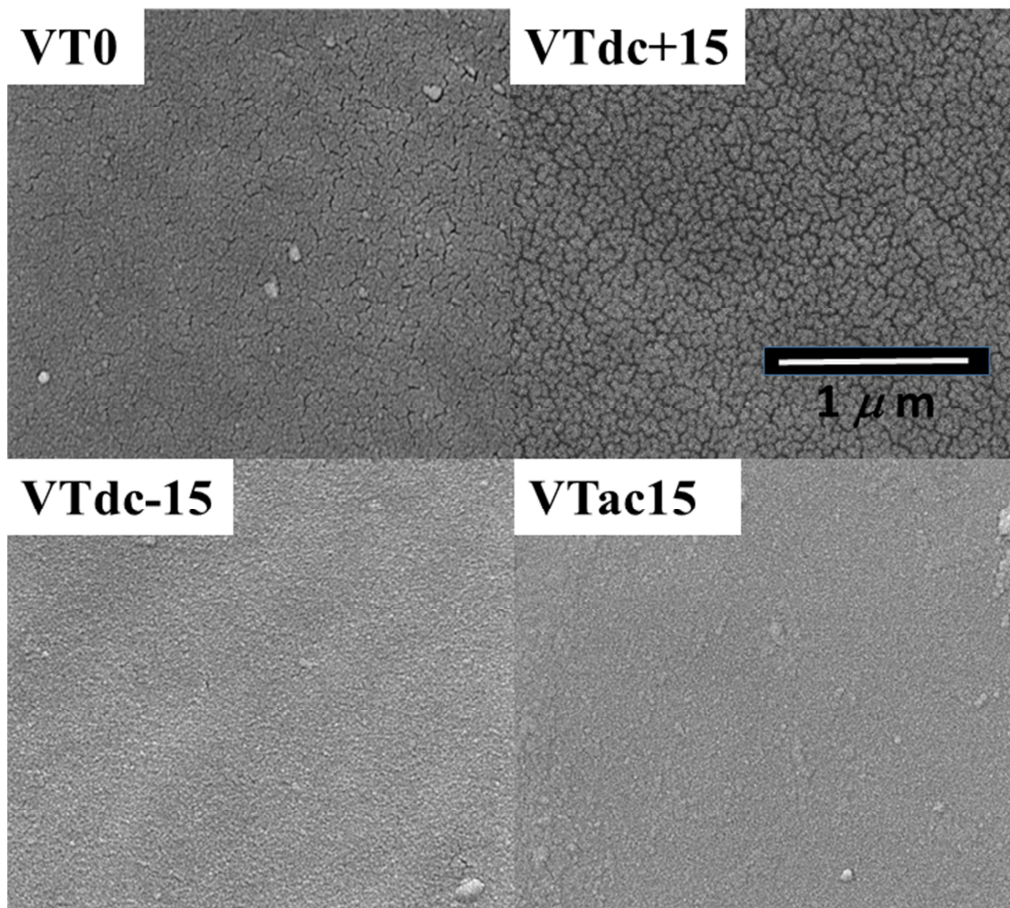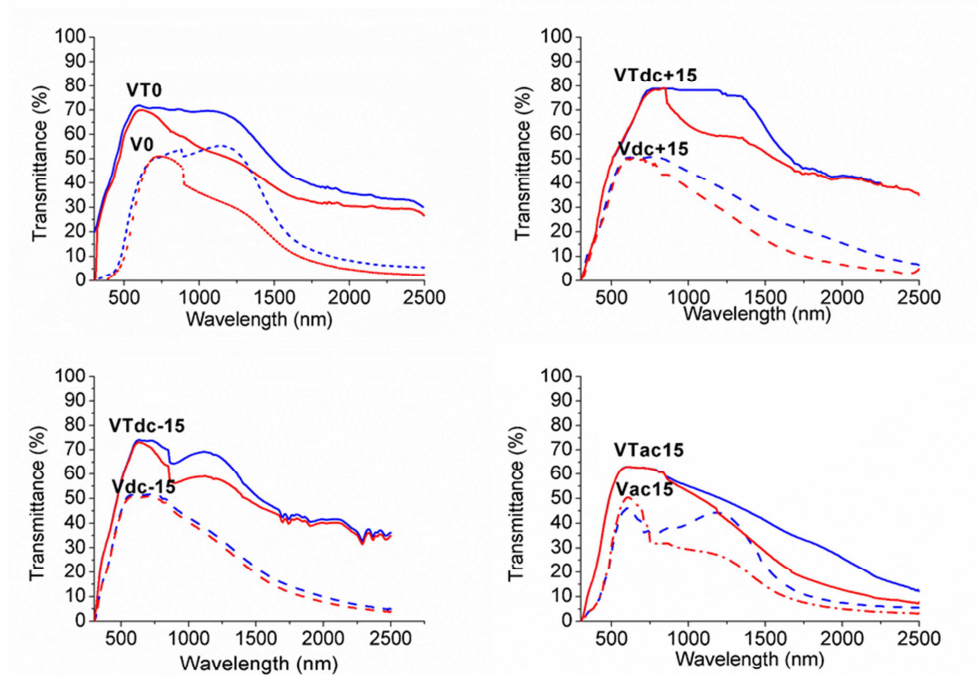

Fig. 2. XRD patterns of bare VO$_2$ and bilayer VO$_2$/TiO$_2$ films. Peaks attributable to VO$_2$ (+), TiO$_2$ (-) and FTO (*) are indicated.

Fig. 3.SEM images of bare VO$_2$ films produced by ElFi-AACVD, under 0 and 1500 V m^{-1} field strengths, with positive DC bias, negative DC bias, and AC.

Fig. 4.SEM images of bilayerVO$_2$/TiO$_2$ films.

Fig. 5. UV-Vis spectra for bare VO_2 (dashed lines) and bilayer VO_2/TiO_2 (solid lines) films at room temperature (blue) and at 80 °C (red).
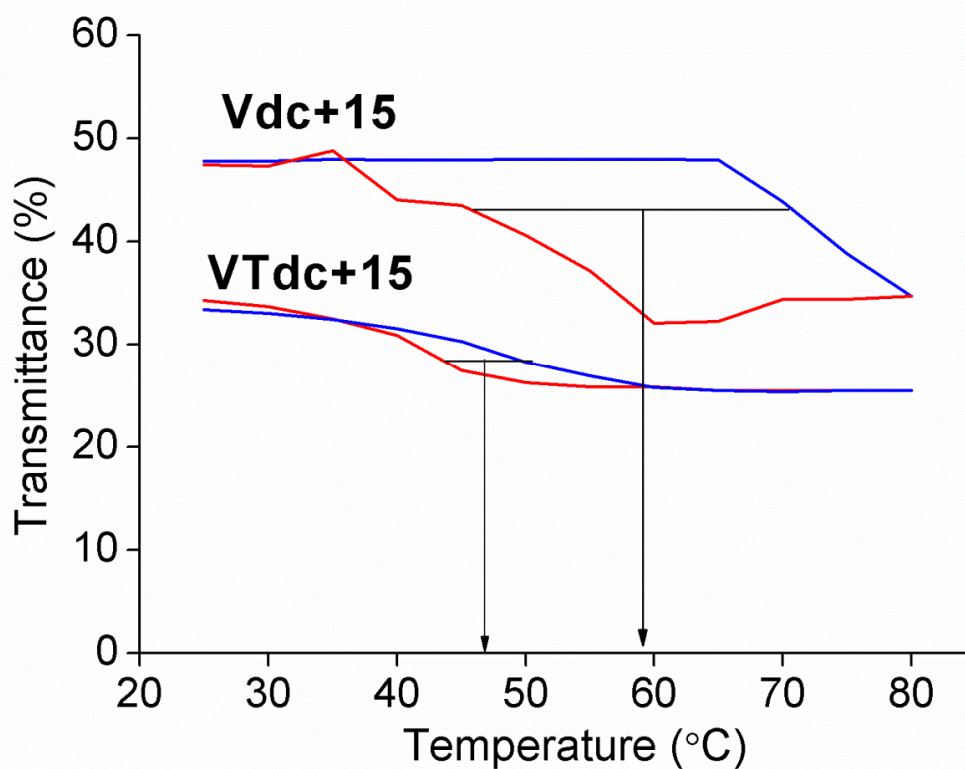
Fig. 6. NIR transmittance hysteresis plots recorded at 1100 nm for Vdc+15 (solid lines) and VTdc+15 (dashed lines) films. Blue and red lines denote heating and cooling runs, respectively. The arrows denote the T_c values.
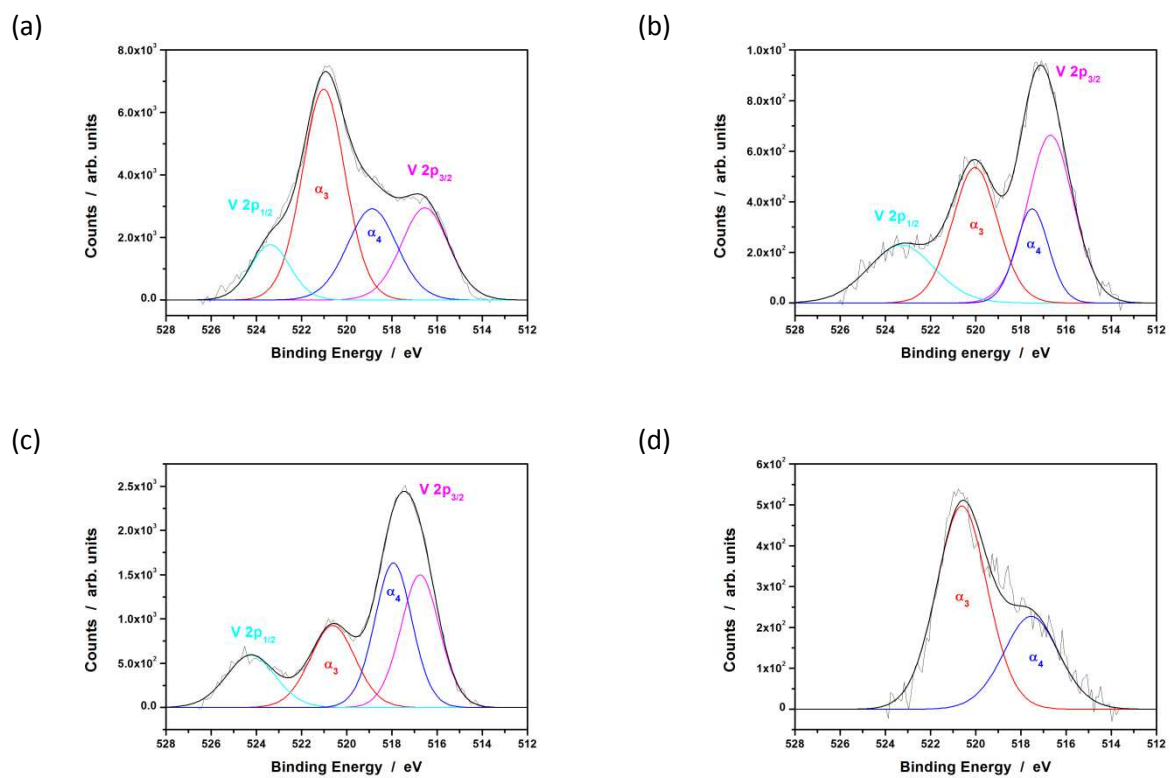
Fig. 7. Fitted vanadium XPS spectra for (a) VT0, (b) VTdc+15, (c) VTdc-15 and (d) VTac15 films. For data representation a Shirley-type background was subtracted.
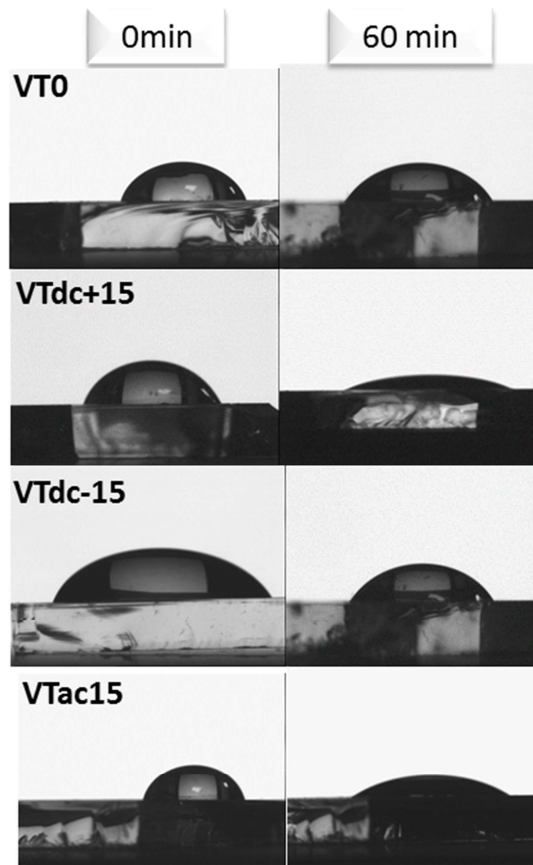
Fig. 8. Images of water droplets on the surface of VO_2/TiO_2 bilayer films before and after 60 min of UV irradiation at 254 nm.